THE JOURNAL OF PHYSICAL CHEMISTRY B

Article

pubs.acs.org/JPCB

Terahertz Chiroptical Spectroscopy of an α-Helical Polypeptide: A Molecular Dynamics Simulation Study

Jun-Ho Choi and Minhaeng Cho*

Department of Chemistry, Korea University, Seoul 136-713, Korea

Supporting Information

ABSTRACT: Vibrational spectroscopy has provided incisive information on the structure of biological molecules. Here, using a molecular dynamics simulation method, infrared vibrational circular dichroism and vibrational optical rotatory dispersion spectra of a right-handed α-helix in the terahertz (THz) frequency range are calculated. Both the autocorrelation function of an electric dipole moment and the cross-correlation function of electric and magnetic dipole moments of the α-helix are calculated and Fourier-transformed to obtain THz absorption and optical activity spectra, which reveal characteristic features of the helical polypeptide structure. The anharmonicity and delocalized nature of the low-frequency modes in the THz frequency domain are taken into account to obtain statistically convergent results on the THz optical activity spectra. In addition, the magnitude of the THz vibrational optical activity signal of the α-helix is directly compared with those of typical, previously studied mid- and near-infrared chiral molecules. We anticipate that THz chiroptical spectroscopy that has not yet been demonstrated experimentally would provide highly important and complementary information on protein structure and dynamics.

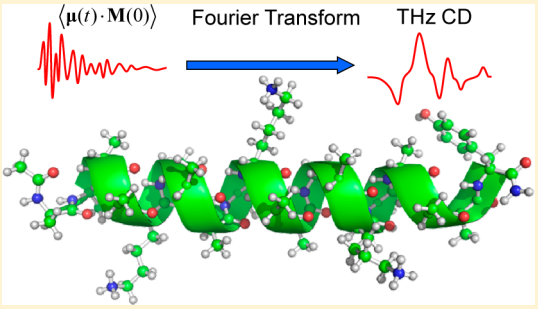

I. INTRODUCTION

Owing to the dramatic advancement in laser technology, a stable and intense terahertz (THz) pulse with a broad spectral bandwidth covering a frequency range from 0.3 to 10 THz is now possible.[1−6] In condensed phases such as solutions, the low-frequency modes of either biological polymers or solvent molecules are the highly collective motions of many atoms in a composite system.[7−9] Over the years, the collective modes of which frequencies of a protein are well within the THz frequency range have been extensively investigated to elucidate an underlying relationship between such large-amplitude collective motions and that protein's function.[2,10−16]

For instance, THz spectroscopy in combination with the femtosecond IR pump−probe measurement method has provided critical information on water structure and dynamics.[17−20] The THz vibrational modes of a lysozyme crystal were recently observed by using an orientation-sensitive THz microscopy technique, which revealed underdamped long-range collective protein vibrations with frequencies larger than 10 cm^{-1}.[21] Turton et al. recently showed that certain THz underdamped vibrational motions, which were detected using the optical Kerr effect measurement method, might govern protein−ligand binding in solution.[22] THz spectroscopy has also been found to be useful in studying solvation dynamics around five-helix bundle λ^*_{6-85} proteins, as demonstrated by Ebbinghaus et al.[18] They also showed that site-specific mutations in a protein cause a notable change in the THz absorption spectrum, which indicates significant restructuring of a protein's hydration shell.[23]

Although THz absorption spectroscopy is undoubtedly useful for probing the structure and dynamics of biological molecules, it has certain limitations. Quantitatively analyzing THz absorption spectra is complicated because of (i) the strong background absorption of water in this frequency region, (ii) a featureless, broad line shape resulting from congestion of low-frequency collective vibrational bands, and (iii) its lack of sensitivity to molecular chirality. Consequently, THz optical activity spectroscopy has been believed to be an important complementary tool to THz absorption spectroscopy, much like the vibrational circular dichroism (VCD) (Raman optical activity) method[24−26] is complementary to IR absorption (Raman scattering) spectroscopy. Water molecules do not contribute to a THz optical activity signal even though water molecules on the surface of a protein may produce an induced THz circular dichroism/optical rotatory dispersion (CD/ORD) signal. Undoubtedly, the THz CD and ORD (TCD and TORD, respectively) spectra of a protein would be highly sensitive to its secondary and tertiary structures. Despite these advantages in THz optical activity spectroscopy, TCD or TORD measurements have not yet become successful because of their extremely weak signals as well as other technical difficulties in precisely manipulating THz pulses and their polarization states.[27−31] Nonetheless, interesting work has been reported by Xu et al., who presented numerical simulation

Received: August 24, 2014
Revised: October 24, 2014
Published: October 24, 2014

dx.doi.org/10.1021/jp508547y | J. Phys. Chem. B 2014, 118, 12837−12843

results of TCD spectra of α-helix and bacteriorhodopsin.[32] The primary aim of their work was to suggest that the THz optical activity measurement method can be of use in searching for evidence of extraterrestrial life in the future. However, they used an overly simple mass and spring model in which atoms are assumed to have the same mass and be connected by harmonic springs; this model resulted in strong and complicated TCD spectra. However, it should be emphasized that these collective low-frequency modes are highly anharmonic and strongly coupled to one another. Furthermore, their frequencies are quite sensitive to protein structure and local electrostatic environment, the latter of which is known as vibrational solvatochromism.[33−35] Furthermore, the transition dipole moments of such low-frequency modes are complicatedly dependent on a protein's backbone structures and intermolecular interactions with surrounding solvent molecules. Therefore, we believe that either quantum chemistry calculations or molecular dynamics (MD) simulations with explicit water molecules are at least required to properly simulate any realistic THz IR and CD/ORD spectra. Over the years, we have developed time-correlation function approaches to the simulations of both linear (IR and VCD) and nonlinear IR pump−probe and two-dimensional IR spectra of a variety of molecules in the frequency range from mid-IR to near-IR regions, which has enabled us to understand fundamental vibrational dynamics, overtone and combination modes, and various coupling-induced processes.[36−45]

In this paper, we present for the first time the TCD and TORD spectra of α-helix in either the gas phase or an aqueous solution. The density functional theory (DFT) calculation of α-helix provides information on the nature of low-frequency modes and IR and THz spectra (section II). However, to fully take into account solvation effects on α-helical structures and to obtain statistically convergent results of simulated IR and TCD (or TORD) spectra, we carried out a sufficiently long MD simulation of α-helix in water and calculated the auto- and cross-correlation functions of the electric and magnetic dipoles. The simulated spectra are discussed in section III. Finally, the main results of the present work are summarized in section IV.

II. QUANTUM CHEMISTRY CALCULATION RESULTS

Alanine, among 20 natural amino acids, is known to have a strong propensity for forming a stable α-helix in an aqueous solution. To increase the water solubility of α-helical polypeptides and to enhance the stability of their secondary structures, charged amino acids like lysine or arginine have been introduced into these alanine-rich polypeptides.[35,46−49] Here, because geometry optimization and vibrational analysis of large polypeptides with more than 20 residues is very expensive and time-consuming, we instead consider a shorter one, *Ac*-(A_4)K(A_4)K-NH_2, for the present quantum chemistry calculation study. Geometry optimization and normal-mode analysis of this α-helix model were performed with the DFT method of B3LYP and the basis set of 6-31G(d) that are implemented in the Gaussian 03 program package.[50] From the vibrational analysis with a scaling factor[51] of 0.9614 for correcting harmonic frequencies, the electric dipole and rotatory strengths of all of the normal modes were obtained, which in turn determined the corresponding IR absorption and VCD (and ORD) intensities, respectively.

In Figure 1, the geometry-optimized structure of the α-helical model *Ac*-(A_4)K(A_4)K-NH_2 is shown, in which the intramolecular hydrogen-bonding interactions are depicted as

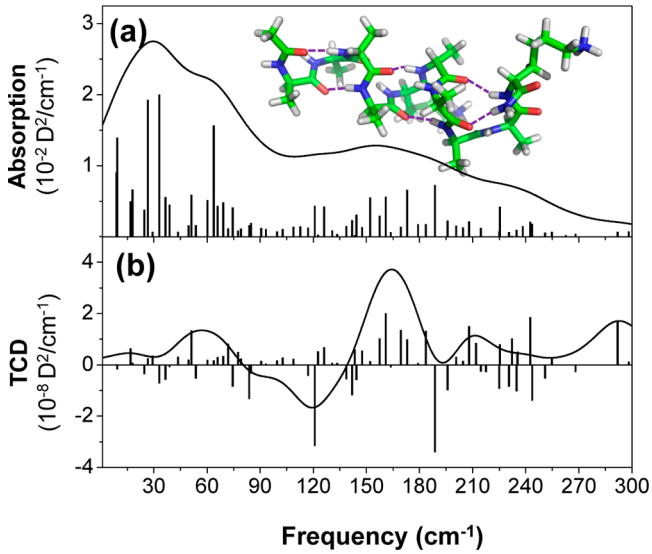

Figure 1. (a) THz absorption and (b) CD spectra of α-helical model *Ac*-(A_4)K(A_4)K-NH_2. Bars represent (a) dipole and (b) rotatory strengths of the corresponding normal modes, respectively. D = Debye. Inset = optimized structure of the α-helix model.

dashed lines. The IR absorption and vibrational CD spectra of this α-helix model in the THz frequency range (10−300 cm^{-1}) are plotted in Figure 1 with the corresponding bar spectra. For simplicity, we assumed that the line shape is given by the Lorentzian function $\gamma/\{(\tilde{\nu} - \tilde{\nu}_0)^2 + \gamma^2\}$ with γ = 20 cm^{-1}. In the THz frequency region, there are a large number of contributing normal modes, and most of them are significantly delocalized over the entire polypeptide. Therefore, it is often difficult to make specific vibrational assignments of such low-frequency modes, unlike the localized normal peaks of high-frequency modes. Recently, Itoh et al. carried out DFT calculations of α-helical alanine polypeptides with 8−24 residues and calculated the corresponding THz absorption spectra.[52] Our calculated THz absorption spectrum is similar to theirs in the frequency region up to 200 cm^{-1}. Notably, they found that as the α-helical chain length increases, the peaks with frequency less than 50 cm^{-1} are red-shifted, whereas the high-frequency modes (>50 cm^{-1}) are blue-shifted. They suggested that vibrational modes with a frequency less than 50 cm^{-1} are mainly bending and twisting modes of the rodlike α-helix (Figure S1, Supporting Information) and could be viewed as acoustic branches of an ideally long α-helical polypeptide.[52] The vibrational modes with a frequency ranging from 50 to 300 cm^{-1} result from the mixing of various bending modes with the peptide backbone and side chain motions.

Although certain spectral structures in the THz absorption spectrum in Figure 1a exist, the TCD spectrum shown in Figure 1b exhibits a significant number of rich spectral features that originate from the distribution of angular components in the THz vibrations. The positive and negative peaks in the TCD spectrum result from constructive and destructive interference between THz-active chiral-mode contributions. The peak intensity ratio of TCD to THz IR absorption, known as the anisotropy or dissymmetry factor defined as $\Delta A/A$, is found to be about 10^{-6} (compare the *y*-axis scales of the two graphs in Figure 1). On the basis of our previous computational studies of VCD and VORD (vibrational ORD) of typical organic chiral molecules in the mid-IR and near-IR frequency regions,[44] we expected that the anisotropy value in the THz

dx.doi.org/10.1021/jp508547y | J. Phys. Chem. B 2014, 118, 12837−12843

region is likely to be $\sim 10^{-6}-10^{-5}$; indeed, the DFT-calculated anisotropy value is in that range. The present quantum chemistry calculations and normal-mode analysis results provide important information on various vibrational properties, such as transition electric and magnetic dipole moments, normal-mode frequencies, corresponding eigenvectors, and so on within the double harmonic approximation. However, due to strong anharmonic couplings and structural fluctuation of an α-helical polypeptide in aqueous solution, the ab initio calculated THz absorption and CD spectra may not fully represent the realistic spectra of α-helix in water, which would be experimentally measured in the future. Thus, we carried out an extensive MD simulation study of our α-helical polypeptide model in water.

III. MD SIMULATION STUDY OF THZ ABSORPTION AND OPTICAL ACTIVITY SPECTRA

A. Computational Details for MD Simulation. The polypeptide considered for the present MD simulation study is *Ac*-(A_4)K(A_4)K(A_4)K(A_4)Y-NH_2, where A = Ala, K = Lys, and Y = Tyr, and in which amino and acid termini are blocked by acetylation (*Ac*) and amidation (NH_2), respectively, to reduce any possible end-fraying effects induced by charged terminal groups. For the sake of a direct comparison with the DFT calculation results, we also carried out classical MD simulations for the same short oligopeptide, *Ac*-(A_4)K(A_4)K-NH_2, considered in section II above. However, due to an insufficient number of intramolecular H-bonds to stabilize the α-helical conformation, population of the helical structure in this case is very low, which has been demonstrated previously.[46] Consequently, for the present MD simulation studies, the longer Ala-rich oligopeptide has been considered. The oligopeptide *Ac*-(A_4)K(A_4)K(A_4)K(A_4)Y-NH_2 is put in a periodic box containing 7632 TIP3P[53] water molecules and three Cl^- anions. The chloride anions were added to the system to neutralize the polypeptide, which contains three positively charged Lys residues. The periodic boundary condition was imposed, and long-range electrostatic interactions were treated by the particle-mesh Ewald method.[54,55] A cutoff distance of 8 Å was used when intermolecular nonbonding interactions were calculated. The composite system was first energy-minimized with the steepest descent and the conjugate gradient methods. Then, a 200 ps NPT ensemble simulation at a constant pressure of 1 atm and temperature of 273 K was performed to adjust the periodic box size. The time step of the MD simulation was set to 1 fs. An additional 200 ps constant NVT simulation at 273 K was performed to thermally equilibrate the entire system. The production run was carried out for 1 ns at NVT conditions, and simulation trajectories, including all of the atomic coordinates, were saved every 100 fs to calculate the THz absorption and CD/ORD spectra of the 20-residue α-helix.

We found that even though a 1 ns simulation is usually sufficient to calculate the THz absorption spectrum, for an accurate calculation of the TCD and TORD spectra, a significantly longer trajectory, or an ensemble of many short trajectories, is needed to increase the signal-to-noise ratio of the extremely weak TCD and TORD spectra. Therefore, we repeated both the 200 ps NVT equilibrium simulation and the 1 ns MD simulation 110 times with a variable set of initial atomic velocities so that the 110 MD-generated trajectories constitute an ensemble of equilibrium trajectories. The time-correlation functions needed to obtain the THz spectra are averaged over the 110 MD trajectories. Before the computational results are presented, it should be noted that after the 200 ps NVT equilibrium simulation, the structure of model peptide *Ac*-(A_4)K(A_4)K(A_4)K(A_4)Y-NH_2 is indeed α-helical as shown in Figure 2 (see Figure S2 in the Supporting Information for more snapshot structures of this α-helical polypeptide taken from the MD trajectories) and that this secondary structure remains stable for each 1 ns simulation time.

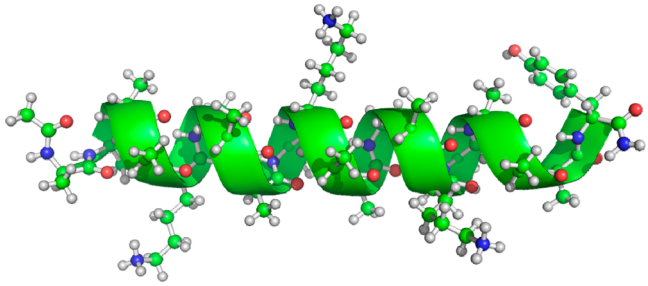

Figure 2. Molecular structure of α-helical *Ac*-(A_4)K(A_4)K(A_4)K(A_4)Y-NH_2, which is taken from the MD-simulation trajectory after the 200 ps NVT equilibrium simulation.

B. Time-Correlation Function. Once the atomic coordinates and polypeptide velocities are saved, calculating the electric and magnetic dipole moments of the α-helical polypeptide is straightforward. Denoting the electric and magnetic dipole moments as $\boldsymbol{\mu}(t)$ and $\mathbf{M}(t)$, respectively, from each 1 ns MD trajectory, and with more than 10000 configurations taken from the trajectory, we calculated the electric and magnetic dipole moments fluctuating in time, which are

$$\boldsymbol{\mu}(t) = \sum_i q_i(t)\mathbf{r}_i(t), \text{ and}$$

$$\mathbf{M}(t) = \frac{1}{2c}\sum_i q_i(t)\mathbf{r}_i(t) \times \mathbf{v}_i(t) \quad (1)$$

Here, $q_i(t)$, $\mathbf{r}_i(t)$, and $\mathbf{v}_i(t)$ represent the atomic partial charge, position vector, and velocity vector of the ith atom in the α-helix, respectively. We used AMBER atomic charges.[54] In ref 44, we used a quantum mechanical/molecular mechanical (QM/MM) MD simulation method to calculate the mid-IR and near-IR absorption and vibrational CD spectra of organic chiral molecules; the chiral molecule was treated quantum mechanically, and the solvent molecules were treated molecular mechanically. In the near-IR frequency region, the polarizable nature of an organic chiral molecule, such as induced electric and magnetic dipoles, is extremely important in quantitatively predicting the near-IR absorption and VCD spectra that reveal the vibrational dynamics and chiroptical properties of overtone and combination modes. On the other hand, mid-IR absorption and VCD spectra are not strongly affected by a polarization effect, such that constant atomic partial charges with a proper QM/MM MD trajectory were sufficient for quantitative prediction of the corresponding vibrational spectra.[44] Therefore, we believe that the electric and magnetic dipole moments that are needed for simulating low-frequency THz vibrational spectra could be calculated with fixed atomic partial charges.

The center of mass for the α-helix was chosen to be the origin of the molecule-fixed coordinate frame. Time-dependent

dx.doi.org/10.1021/jp508547y | J. Phys. Chem. B 2014, 118, 12837−12843

electric and magnetic dipole moment trajectories are used to calculate the autocorrelation function of the electric dipole and the cross-correlation function of the electric and magnetic dipoles. The IR absorption ($A(\omega)$) and VCD ($\Delta A(\omega)$) spectra are then the Fourier transforms of the respective time-correlation functions[56,57]

$$A(\omega) \propto \int_{-\infty}^{\infty} dt e^{i\omega t} \langle \boldsymbol{\mu}(t)\cdot\boldsymbol{\mu}(0)\rangle, \text{ and} \tag{2}$$

$$\Delta A(\omega) \equiv A_{\mathrm{L}}(\omega) - A_{\mathrm{R}}(\omega) \propto \mathrm{Im} \int_{-\infty}^{\infty} dt e^{i\omega t} \langle \boldsymbol{\mu}(t)\cdot\mathbf{M}(0)\rangle \tag{3}$$

where $A_{\mathrm{L}}(\omega)$ and $A_{\mathrm{R}}(\omega)$ represent the absorption spectrum measured by employing left- and right-circularly polarized THz radiation, respectively.

The calculated time-correlation functions $\langle \boldsymbol{\mu}(t)\cdot\boldsymbol{\mu}(0)\rangle$ and $\langle \boldsymbol{\mu}(t)\cdot\mathbf{M}(0)\rangle$, averaged over independent MD trajectories, are plotted in Figure 3a and 3b, respectively. Here, D and μ_{B} represent Debye and Bohr magnetons, respectively. The electric dipole autocorrelation function $\langle \boldsymbol{\mu}(t)\cdot\boldsymbol{\mu}(0)\rangle$ decays monotonically. On the other hand, the ensemble average cross-correlation function $\langle \boldsymbol{\mu}(t)\cdot\mathbf{M}(0)\rangle$ (black line, Figure 3b) exhibits highly oscillating features. In ref 56, we showed that if the equality condition $\langle \boldsymbol{\mu}(t)\cdot\mathbf{M}(0)\rangle = -\langle \boldsymbol{\mu}(0)\cdot\mathbf{M}(t)\rangle$ holds, the calculated cross-correlation function $\langle \boldsymbol{\mu}(t)\cdot\mathbf{M}(0)\rangle$ can be considered as converged. Note that the cross-correlation function $\langle \boldsymbol{\mu}(t)\cdot\mathbf{M}(0)\rangle$ has a time-odd property due to the time-reversal, antisymmetric magnetic dipole moment. In an ideal case, the cross-correlation function $\langle \boldsymbol{\mu}(0)\cdot\mathbf{M}(t)\rangle$ should symetrically mirror $\langle \boldsymbol{\mu}(t)\cdot\mathbf{M}(0)\rangle$ in magnitude. However, the calculated $\langle \boldsymbol{\mu}(t)\cdot\mathbf{M}(0)\rangle$ appears to be slightly different from $-\langle \boldsymbol{\mu}(0)\cdot\mathbf{M}(t)\rangle$. Nevertheless, the general oscillating patterns are quite similar to each other. The blue line in Figure 3b is the sum of $\langle \boldsymbol{\mu}(t)\cdot\mathbf{M}(0)\rangle$ and $\langle \boldsymbol{\mu}(0)\cdot\mathbf{M}(t)\rangle$, which in an ideal case would vanish. The slowly varying aspect of functions $\langle \boldsymbol{\mu}(t)\cdot\mathbf{M}(0)\rangle$ and $\langle \boldsymbol{\mu}(0)\cdot\mathbf{M}(t)\rangle$, which is not shown in Figure 3b, is also different. However, it should be noted that the high-oscillating features in the two cross-correlation functions have necessary information on THz CD/ORD contributions from all of the low-frequency vibrational modes.

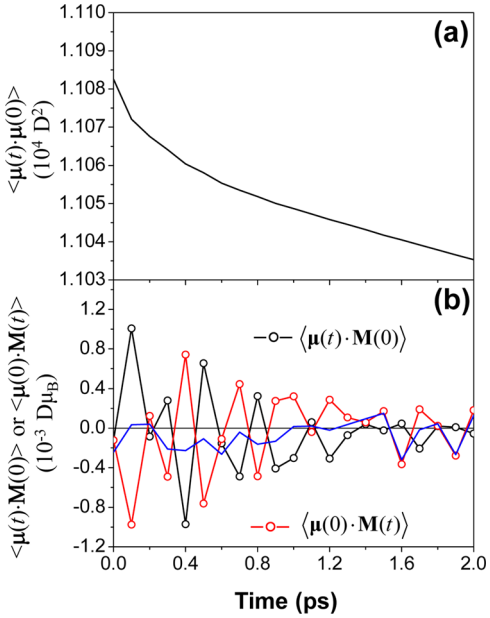

Figure 3. Time-correlation functions $\langle \boldsymbol{\mu}(t)\cdot\boldsymbol{\mu}(0)\rangle$, $\langle \boldsymbol{\mu}(t)\cdot\mathbf{M}(0)\rangle$, and $\langle \boldsymbol{\mu}(0)\cdot\mathbf{M}(t)\rangle$. The dimensions of $\langle \boldsymbol{\mu}(t)\cdot\boldsymbol{\mu}(0)\rangle$ and $\langle \boldsymbol{\mu}(t)\cdot\mathbf{M}(0)\rangle$ are D^2 and $\mathrm{D}\mu_{\mathrm{B}}$, respectively, where μ_{B} = Bohr magneton. The blue line is the sum of the two correlation functions: black line = $\langle \boldsymbol{\mu}(t)\cdot\mathbf{M}(0)\rangle$, and red line = $\langle \boldsymbol{\mu}(0)\cdot\mathbf{M}(t)\rangle$.

C. THz Absorption and CD Spectra. Although the MD simulation faithfully reflects vibrational dynamics of molecules in condensed phases, vibrational lifetime broadening cannot be properly taken into account in the time-correlation-function approaches that are based on thermal equilibrium MD simulations. Here, it is assumed that the vibrational lifetime broadening is approximately accounted for by multiplying the exponentially decaying function $\exp(-t/2T_1)$, with T_1 = 500 fs, to the calculated ensemble average time-correlation functions. Then, Fourier-transforming the auto- and cross-correlation functions gives us the THz IR and TCD/TORD spectra. The frequency range of the spectra is in this case determined by the time step of the MD simulation. For instance, saving the MD trajectory every 4 fs can be used to obtain a mid-IR spectrum with a frequency range from 0 to ~2000 cm^{-1}. Saving the coordinate files at every 1 fs provides the simulated spectrum near-IR overtone and combination-mode transitions with frequencies up to 6000 cm^{-1}. With the Nyquist critical frequency[58] f_c given as $1/(2\Delta_t)$, with the time step Δ_t = 100 fs, in the present work, the upper frequency bound of the numerically simulated THz absorption and CD spectra is about 170 cm^{-1}. In Figure 4, the THz IR absorption, TCD, and TORD spectra are plotted in the frequency range from 20 to 170 cm^{-1}. The low-frequency (<20 cm^{-1}) region of the THz optical activity spectra is not shown here because the signal-to-

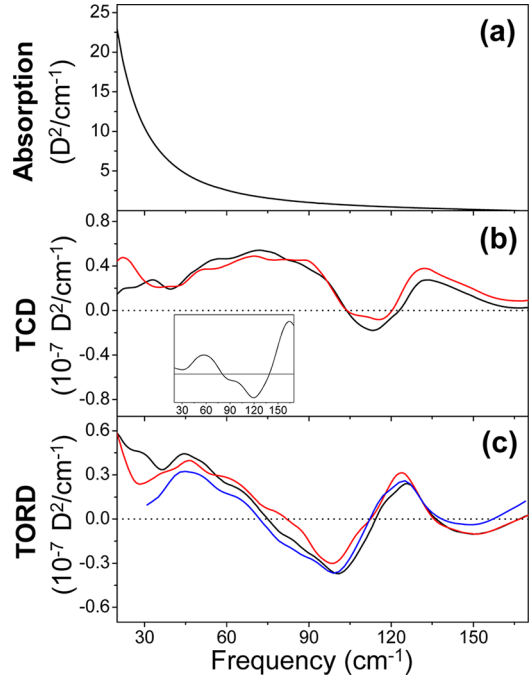

Figure 4. Numerically simulated THz absorption, TCD, and TORD spectra of the α-helix model. (a) The plotted THz absorption spectrum. (b) TCD and (c) TORD spectra obtained from cross-correlation functions $\langle \boldsymbol{\mu}(t)\cdot\mathbf{M}(0)\rangle$ (black line) and $\langle \boldsymbol{\mu}(0)\cdot\mathbf{M}(t)\rangle$ (red line). The TORD spectrum (blue line) obtained by carrying out the Kramers–Kronig (K–K) transformation of the TCD spectrum in (b) is also plotted in (c) for the sake of comparison.

dx.doi.org/10.1021/jp508547y | J. Phys. Chem. B 2014, 118, 12837–12843

noise ratios of such low-frequency TCD and TORD bands are poor, which is due to a lack of convergence in the $\boldsymbol{\mu}-\mathbf{M}$ cross-correlation function obtained even with 110 independent 1 ns MD trajectories.

The THz absorption spectrum in Figure 4a shows a featureless decaying pattern with respect to vibrational frequency, unlike that of the short α-helical polypeptide model (Figure 1a). In contrast, the TCD spectra (Figure 4b) obtained from the Fourier transformations of $\langle\boldsymbol{\mu}(t)\cdot\mathbf{M}(0)\rangle$ and $\langle\boldsymbol{\mu}(0)\cdot\mathbf{M}(t)\rangle$ show interesting (+,−,+) peaks at around 75, 115, and 135 cm^{-1}, respectively. Note that even though the two spectra from $\langle\boldsymbol{\mu}(t)\cdot\mathbf{M}(0)\rangle$ and $\langle\boldsymbol{\mu}(0)\cdot\mathbf{M}(t)\rangle$ are not perfectly the same due to statistical error in calculating the ensemble averages of the corresponding cross-correlation functions, the general TCD line shapes and peak intensities are in quantitative agreement with each other. It is believed that the discrepancy in the two cross-correlation functions primarily causes differences in the spectral background and line shape in the very low-frequency (<20 cm^{-1}) range of the TCD and TORD spectra.

The TCD spectral line shape shown in Figure 4b is an important chiroptical feature of the α-helical polypeptide that results from its collective modes in liquid water. The positive TCD peak in the frequency range from 20 to 60 cm^{-1} is mainly from bending and torsional motions of the helical rod according to normal-mode analysis using the DFT calculation method. In fact, a positive TCD peak also appears in the DFT-calculated TCD spectrum (inset, Figure 4b, which is the DFT-TCD spectrum from Figure 1b with its frequency axis rescaled for direct comparison with the MD-TCD spectrum). Now, the vibrational modes in the frequency range from 60 to 170 cm^{-1} exhibit an alternating sign pattern (+,−,+), and the contributing modes are delocalized vibrations comprised of bending motions mixed with peptide backbone and side chain modes. Such a TCD peak pattern (+,−,+) is also observed in the DFT-TCD spectrum (see peaks from 40 to 180 cm^{-1}). Thus, the overall TCD spectral line shapes in the DFT-TCD and MD-TCD spectra are similar, but due to the solvation-induced frequency shift, the MD-TCD peaks might be red-shifted in comparison to those in the DFT-TCD spectrum. From the calculated $\boldsymbol{\mu}-\mathbf{M}$ cross-correlation functions, we could obtain the TORD spectrum.[59] In Figure 4c, the calculated TORD spectra with $\langle\boldsymbol{\mu}(t)\cdot\mathbf{M}(0)\rangle$ and $\langle\boldsymbol{\mu}(0)\cdot\mathbf{M}(t)\rangle$ are depicted, and they both show the same spectral features, which are (+,−,+,−) peaks at around 45, 100, 125, and 150 cm^{-1}, respectively. Although the TCD and TORD spectra (black line) in Figure 4b and 4c were obtained directly from the real and imaginary parts of the Fourier transformation of the electric dipole-magnetic dipole cross-correlation function, they are in principle related to each other by the Kramers−Kronig (K−K) transformation. More specifically, molar ellipticity $[\theta(\omega')]$ is related to molar rotation $[\varphi(\omega)]$ as

$$[\phi(\omega)] = \frac{2}{\pi}\int_0^\infty \frac{\omega'[\theta(\omega')]}{\omega'^2 - \omega^2}\,d\omega' \tag{4}$$

Because the spectral range of our molar ellipticity (or TCD) spectrum in Figure 4b is from ∼10 to ∼170 cm^{-1}, not from 0 to infinity, the K−K-transformed TORD spectrum (blue line in Figure 4c) should be viewed as an approximation. Nonetheless, the K−K-transformed TORD spectrum is in good agreement with the TORD spectrum (black line) taken from the Fourier transformation of the corresponding time-correlation function.

Next, the peak intensities of the THz absorption bands are compared with those of the THz CD bands. The THz absorption intensities of the collective modes (30 $cm^{-1} < \omega <$ 150 cm^{-1}) vary from 10 to 0.1 D^2/cm^{-1}. The corresponding THz CD peak intensities are in the range from -0.2×10^{-7} to 0.5×10^{-7} D^2/cm^{-1} in the same frequency region. Therefore, the anisotropy ratio ($\Delta A/A$) in the THz frequency region is about $10^{-8}-10^{-7}$. The primary reason that the average anisotropy value of these THz vibrational modes is so small is not because the average rotatory strength is small, but because the average dipole strength of the α-helical polypeptide is unusually large. For the sake of comparison, let us consider the IR absorption and VCD intensity of a typical organic chiral molecule, (1*S*)-(−)-β-pinene, which is studied in detail in ref 44 using the QM/MM MD method in combination with a time-correlation function approach. We found that the mid-IR absorption intensities of the fundamental transition modes of (1*S*)-(−)-β-pinene vary from 1×10^{-5} to 4×10^{-5} D^2/cm^{-1}, whereas the corresponding VCD intensities range from -2×10^{-9} to 2×10^{-9} D^2/cm^{-1}. Consequently, the anisotropy value ($\Delta A/A$) of (1*S*)-(−)-β-pinene is about 10^{-4}, which is fully consistent with experimental results.[44] The TCD intensity of 0.4×10^{-7} D^2/cm^{-1} for the present α-helical polypeptide is in fact much larger than that of (1*S*)-(−)-β-pinene. However, due to the large dipole strength of the THz vibrational modes of the α-helical polypeptide, the anisotropy, which is the relative TCD intensity with respect to the THz absorption intensity, is very small. This is a counterintuitive result because low-frequency vibrational modes are expected to have a much smaller angular moment component in their vibrations due to their large reduced masses. However, the present simulation study shows that the angular component and magnetic dipole moments are sufficiently large for those THz vibrational modes, but that the linear vibrations and associated changes in the electric dipole moment are also very large, which makes the anisotropy value small in comparison to those of mid-IR and near-IR vibrational modes.

Now, we present a discussion on how solvent water affects the THz chiroptical signals of the collective low-frequency vibrational modes of an α-helical polypeptide. As shown in ref 18, water molecules in the hydration shell of a protein enhance the THz absorption (but not TCD) signal. It was shown that the THz (3−6 THz domain) absorption coefficient of lysozyme in a crystalline form increases as the protein becomes more hydrated.[60] Thus, water molecules around a protein may also enhance TCD signals, or the corresponding rotational strengths, associated with the delocalized vibrational modes.[32] It will be highly interesting to study such hydration effects on the TCD intensities of low-frequency modes of proteins in the future. Second, there is another complication that could not be studied in the present work. Although achiral water molecules produce no TCD or TORD signals in bulk water, the finiteness of the periodic box size considered in the present MD simulations means that the overall TCD signals originating from certain water molecules on the surface of the box are not negligible, fluctuate widely in time, and do not vanish even after taking an average over the entire 110 ns simulation trajectories.[61] Furthermore, those water molecules in the vicinity of the α-helical polypeptide would acquire chirality due to their interactions with structurally chiral polypeptides. Therefore, the induced TCD and TORD of water molecules in the first few hydration shells around the α-helix could also contribute to the experimentally measured spectrum. Currently, these issues are being investigated by carrying out much longer simulations with a significantly larger periodic box and

polarizable water-potential models. Nonetheless, the general TCD spectral line shapes shown in Figures 1b and 4b are believed to be generalizable and characteristic of an α-helical polypeptide, which in turn reveals the nature of chiral angular oscillations of low-frequency, delocalized α-helix modes.

IV. SUMMARY

In the present study, we presented for the first time numerically simulated TCD and TORD spectra of an α-helical polypeptide in water using both an MD simulation method and a time-correlation function approach. In the THz frequency domain ($30\ cm^{-1} < \omega < 170\ cm^{-1}$), the TCD spectrum of *Ac*-$(A_4)K(A_4)K(A_4)K(A_4)Y$-NH_2 in water exhibits a characteristic positive peak for low-frequency bending modes and (+,−,+) peaks of mixed bending, peptide backbone, and side chain modes. Here, it was shown that the convergence test can be performed by comparing the two TCD spectra obtained from time-odd $\boldsymbol{\mu}-\mathbf{M}$ cross-correlation functions in both positive and negative time domains. The rotatory strengths of the THz-active modes of the α-helical polypeptide are fairly strong; the TCD intensity can be as large as $0.5 \times 10^{-7}\ D^2/cm^{-1}$. We anticipate that the present work and computational approaches will be of great use for future experimental developments in TCD and TORD measurement methods, and for applications to studies of not only low-frequency, large-amplitude vibrational motions of proteins but also their possible relationship with protein function in the future.

■ ASSOCIATED CONTENT

Ⓢ Supporting Information

Atomic displacement vector representations of low-frequency normal-mode eigenvectors of DFT-calculated *Ac*-$(A_4)K(A_4)K$-NH_2 and a few representative conformations of *Ac*-$(A_4)K(A_4)$-$K(A_4)K(A_4)Y$-NH_2 taken from MD trajectories. This material is available free of charge via the Internet at http://pubs.acs.org.

■ AUTHOR INFORMATION

Corresponding Author

*E-mail: mcho@korea.ac.kr. Tel: +82-2-3290-3133. Fax: +82-2-3290-3121.

Notes

The authors declare no competing financial interest.

■ ACKNOWLEDGMENTS

This work was supported by National Research Foundation of Korea (NRF) grants funded by the Korean government (MEST) (Grants 20110020033 and 2013013156) and by the Samsung Science & Technology Foundation (SSTF-BA1401-12). J.-H.C. acknowledges financial support from a Korea University Grant and the NRF fund (2013061203).

■ REFERENCES

(1) Nahata, A.; Weling, A. S.; Heinz, T. F. A Wideband Coherent Terahertz Spectroscopy System Using Optical Rectification and Electro-Optic Sampling. *Appl. Phys. Lett.* **1996**, *69*, 2321−2323.
(2) Markelz, A. G.; Roitberg, A.; Heilweil, E. J. Pulsed Terahertz Spectroscopy of DNA, Bovine Serum Albumin and Collagen between 0.1 and 2.0 THz. *Chem. Phys. Lett.* **2000**, *320*, 42−48.
(3) Schmuttenmaer, C. A. Exploring Dynamics in the Far-Infrared with Terahertz Spectroscopy. *Chem. Rev.* **2004**, *104*, 1759−1780.
(4) Hebling, J.; Yeh, K.-L.; Hoffmann, M. C.; Bartal, B.; Nelson, K. A. Generation of High-Power Terahertz Pulses by Tilted-Pulse-Front Excitation and Their Application Possibilities. *J. Opt. Soc. Am. B* **2008**, *25*, B6−B19.
(5) Kampfrath, T.; Tanaka, K.; Nelson, K. A. Resonant and Nonresonant Control over Matter and Light by Intense Terahertz Transients. *Nat. Photonics* **2013**, *7*, 680−690.
(6) Liu, M.; Hwang, H. Y.; Tao, H.; Strikwerda, A. C.; Fan, K.; Keiser, G. R.; Sternbach, A. J.; West, K. G.; Kittiwatanakul, S.; Lu, J.; et al. Terahertz-Field-Induced Insulator-to-Metal Transition in Vanadium Dioxide Metamaterial. *Nature* **2012**, *487*, 345−348.
(7) Brooks, B.; Karplus, M. Harmonic Dynamics of Proteins: Normal Modes and Fluctuations in Bovine Pancreatic Trypsin Inhibitor. *Proc. Natl. Acad. Sci. U.S.A.* **1983**, *80*, 6571−6575.
(8) Go, N.; Noguti, T.; Nishikawa, T. Dynamics of a Small Globular Protein in Terms of Low-Frequency Vibrational Modes. *Proc. Natl. Acad. Sci. U.S.A.* **1983**, *80*, 3696−3700.
(9) Levitt, M.; Sander, C.; Stern, P. S. Protein Normal-Mode Dynamics: Trypsin Inhibitor, Crambin, Ribonuclease and Lysozyme. *J. Mol. Biol.* **1985**, *181*, 423−447.
(10) Zhang, C.; Tarhan, E.; Ramdas, A. K.; Weiner, A. M.; Durbin, S. M. Broadened Far-Infrared Absorption Spectra for Hydrated and Dehydrated Myoglobin. *J. Phys. Chem. B* **2004**, *108*, 10077−10082.
(11) Whitmire, S. E.; Wolpert, D.; Markelz, A. G.; Hillebrecht, J. R.; Galan, J.; Birge, R. R. Protein Flexibility and Conformational State: A Comparison of Collective Vibrational Modes of Wild-Type and D96N Bacteriorhodopsin. *Biophys. J.* **2003**, *85*, 1269−1277.
(12) Markelz, A.; Whitmire, S.; Hillebrecht, J.; Birge, R. THz Time Domain Spectroscopy of Biomolecular Conformational Modes. *Phys. Med. Biol.* **2002**, *47*, 3797−3805.
(13) Globus, T. R.; Woolard, D. L.; Khromova, T.; Crowe, T. W.; Bykhovskaia, M.; Gelmont, B. L.; Hesler, J.; Samuels, A. C. THz-Spectroscopy of Biological Molecules. *J. Biol. Phys.* **2003**, *29*, 89−100.
(14) Heyden, M.; Havenith, M. Combining THz Spectroscopy and MD Simulations to Study Protein-Hydration Coupling. *Methods* **2010**, *52*, 74−83.
(15) Sushko, O.; Dubrovka, R.; Donnan, R. S. Terahertz Spectral Domain Computational Analysis of Hydration Shell of Proteins with Increasingly Complex Tertiary Structure. *J. Phys. Chem. B* **2013**, *117*, 16486−16492.
(16) Balu, R.; Zhang, H.; Zukowski, E.; Chen, J. Y.; Markelz, A. G.; Gregurick, S. K. Terahertz Spectroscopy of Bacteriorhodopsin and Rhodopsin: Similarities and Differences. *Biophys. J.* **2008**, *94*, 3217−3226.
(17) Ronne, C.; Thrane, L.; Åstrand, P.-O.; Wallqvist, A.; Mikkelsen, K. V.; Keiding, S. R. Investigation of the Temperature Dependence of Dielectric Relaxation in Liquid Water by THz Reflection Spectroscopy and Molecular Dynamics Simulation. *J. Chem. Phys.* **1997**, *107*, 5319−5331.
(18) Ebbinghaus, S.; Kim, S. J.; Heyden, M.; Yu, X.; Heugen, U.; Gruebele, M.; Leitner, D. M.; Havenith, M. An Extended Dynamical Hydration Shell around Proteins. *Proc. Natl. Acad. Sci. U.S.A.* **2007**, *104*, 20749−20752.
(19) Heugen, U.; Schwaab, G.; Bründermann, E.; Heyden, M.; Yu, X.; Leitner, D. M.; Havenith, M. Solute-Induced Retardation of Water Dynamics Probed Directly by Terahertz Spectroscopy. *Proc. Natl. Acad. Sci. U.S.A.* **2006**, *103*, 12301−12306.
(20) Tielrooij, K. J.; Garcia-Araez, N.; Bonn, M.; Bakker, H. J. Cooperativity in Ion Hydration. *Science* **2010**, *328*, 1006−1009.
(21) Acbas, G.; Niessen, K. A.; Snell, E. H.; Markelz, A. G. Optical Measurements of Long-Range Protein Vibrations. *Nat. Commun.* **2014**, *5*, 3076 DOI: 10.1038/ncomms4076.
(22) Turton, D. A.; Senn, H. M.; Harwood, T.; Lapthorn, A. J.; Ellis, E. M.; Wynne, K. Terahertz Underdamped Vibrational Motion Governs Protein-Ligand Binding in Solution. *Nat. Commun.* **2014**, *5*, 3999 DOI: 10.1038/ncomms4999.
(23) Ebbinghaus, S.; Kim, S. J.; Heyden, M.; Yu, X.; Gruebele, M.; Leitner, D. M.; Havenith, M. Protein Sequence- and pH-Dependent Hydration Probed by Terahertz Spectroscopy. *J. Am. Chem. Soc.* **2008**, *130*, 2374−2375.

(24) *Comprehensive Chiroptical Spectroscopy*; Berova, N., Polavarapu, P., Nakanishi, K., Woody, R. W., Eds.; John Wiley & Sons: Hoboken, NJ, 2012; *Vol. 1*.
(25) Nafie, L. A. *Vibrational Optical Activity: Principles and Applications*; Wiley: New York, 2011.
(26) Barron, L. D. *Molecular Light Scattering and Optical Activity*; Cambridge University Press: New York, 2004.
(27) Castro-Camus, E.; Lloyd-Hughes, J.; Johnston, M. B.; Fraser, M. D.; Tan, H. H.; Jagadish, C. Polarization-Sensitive Terahertz Detection by Multicontact Photoconductive Receivers. *Appl. Phys. Lett.* **2005**, *86*, 254102.
(28) Sato, M.; Higuchi, T.; Kanda, N.; Konishi, K.; Yoshioka, K.; Suzuki, T.; Misawa, K.; Kuwata-Gonokami, M. Terahertz Polarization Pulse Shaping with Arbitrary Field Control. *Nat. Photonics* **2013**, *7*, 724−731.
(29) Yasumatsu, N.; Watanabe, S. Precise Real-Time Polarization Measurement of Terahertz Electromagnetic Waves by a Spinning Electro-Optic Sensor. *Rev. Sci. Instrum.* **2012**, *83*, 023104.
(30) Castro-Camus, E. Polarization-Resolved Terahertz Time-Domain Spectroscopy. *J. Infrared, Millimeter, Terahertz Waves* **2012**, *33*, 418−430.
(31) Xu, J.; Plaxco, K. W.; Allen, S. J. THz Spectroscopy of Proteins in Water: Direct Absorption and Circular Dichroism. *Int. J. High Speed Electron. Syst.* **2007**, *17*, 709−718.
(32) Xu, J.; Ramian, G. J.; Galan, J. F.; Savvidis, P. G.; Scopatz, A. M.; Birge, R. R.; Allen, S. J.; Plaxco, K. W. Terahertz Circular Dichroism Spectroscopy: A Potential Approach to the in Situ Detection of Life's Metabolic and Genetic Machinery. *Astrobiology* **2003**, *3*, 489−504.
(33) Kim, H.; Cho, M. Infrared Probes for Studying the Structure and Dynamics of Biomolecules. *Chem. Rev.* **2013**, *113*, 5817−5847.
(34) Cho, M. Vibrational Solvatochromism and Electrochromism: Coarse-Grained Models and Their Relationships. *J. Chem. Phys.* **2009**, *130*, 094505.
(35) Shoemaker, K. R.; Kim, P. S.; York, E. J.; Stewart, J. M.; Baldwin, R. L. Tests of the Helix Dipole Model for Stabilization of Alpha-Helices. *Nature* **1987**, *326*, 563−567.
(36) Cho, M. Coherent Two-Dimensional Optical Spectroscopy. *Chem. Rev.* **2008**, *108*, 1331−1418.
(37) Choi, J.-H.; Hahn, S.; Cho, M. Amide I IR, VCD, and 2D IR Spectra of Isotope-Labeled α-Helix in Liquid Water: Numerical Simulation Studies. *Int. J. Quantum Chem.* **2005**, *104*, 616−634.
(38) Choi, J.-H.; Lee, H.; Lee, K.-K.; Hahn, S.; Cho, M. Computational Spectroscopy of Ubiquitin: Comparison between Theory and Experiments. *J. Chem. Phys.* **2007**, *126*, 045102.
(39) Choi, J.-H.; Raleigh, D.; Cho, M. Azido Homoalanine Is a Useful Infrared Probe for Monitoring Local Electrostatistics and Side-Chain Solvation in Proteins. *J. Phys. Chem. Lett.* **2011**, *2*, 2158−2162.
(40) Hahn, S.; Ham, S.; Cho, M. Simulation Studies of Amide I IR Absorption and Two-Dimensional IR Spectra of Beta Hairpins in Liquid Water. *J. Phys. Chem. B* **2005**, *109*, 11789−11801.
(41) Jeon, J.; Yang, S.; Choi, J.-H.; Cho, M. Computational Vibrational Spectroscopy of Peptides and Proteins in One and Two Dimensions. *Acc. Chem. Res.* **2009**, *42*, 1280−1289.
(42) Kwac, K.; Cho, M. Molecular Dynamics Simulation Study of N-Methylacetamide in Water. I. Amide I Mode Frequency Fluctuation. *J. Chem. Phys.* **2003**, *119*, 2247−2255.
(43) Kwac, K.; Cho, M. Molecular Dynamics Simulation Study of N-Methylacetamide in Water. II. Two-Dimensional Infrared Pump-Probe Spectra. *J. Chem. Phys.* **2003**, *119*, 2256−2263.
(44) Choi, J.-H.; Cho, M. Direct Calculations of Mid- and near-IR Absorption and Circular Dichroism Spectra of Chiral Molecules Using QM/MM Molecular Dynamics Simulation Method. *J. Chem. Theory Comput.* **2011**, *7*, 4097−4103.
(45) Tanimura, Y.; Ishizaki, A. Modeling, Calculating, and Analyzing Multidimensional Vibrational Spectroscopies. *Acc. Chem. Res.* **2009**, *42*, 1270−1279.
(46) Vila, J. A.; Ripoll, D. R.; Scheraga, H. A. Physical Reasons for the Unusual Alpha-Helix Stabilization Afforded by Charged or Neutral Polar Residues in Alanine-Rich Peptides. *Proc. Natl. Acad. Sci. U.S.A.* **2000**, *97*, 13075−13079.
(47) Marqusee, S.; Robbins, V. H.; Baldwin, R. L. Unusually Stable Helix Formation in Short Alanine-Based Peptides. *Proc. Natl. Acad. Sci. U.S.A.* **1989**, *86*, 5286−5290.
(48) Scholtz, J. M.; York, E. J.; Stewart, J. M.; Baldwin, R. L. A Neutral, Water-Soluble, Alpha-Helical Peptide: The Effect of Ionic Strength on the Helix-Coil Equilibrium. *J. Am. Chem. Soc.* **1991**, *113*, 5102−5104.
(49) Fang, C.; Wang, J.; Kim, Y. S.; Charnley, A. K.; Barber-Armstrong, W.; Smith, A. B., III; Decatur, S. M.; Hochstrasser, R. M. Two-Dimensional Infrared Spectroscopy of Isotopomers of an Alanine Rich Alpha-Helix. *J. Phys. Chem. B* **2004**, *108*, 10415−10427.
(50) Frisch, M. J.; Trucks, G. W.; Schlegel, H. B.; Scuseria, G. E.; Robb, M. A.; Cheeseman, J. R.; Montgomery, J. A., Jr.; Vreven, T.; Kudin, K. N.; Burant, J. C.; et al. *Gaussian 03*; Gaussian, Inc.: Wallingford, CT, 2004.
(51) Scott, A. P.; Radom, L. Harmonic Vibrational Frequencies: An Evaluation of Hartree-Fock, Møller-Plesset, Quadratic Configuration Interaction, Density Functional Theory, and Semiempirical Scale Factors. *J. Phys. Chem.* **1996**, *100*, 16502−16513.
(52) Itoh, K.; Ikeda, A.; Iwamoto, T.; Nishizawa, S. DFT Calculation Analysis of Terahertz Time-Domain Spectra of Polyalanines. *J. Mol. Struct.* **2011**, *1006*, 52−58.
(53) Jorgensen, W. L.; Chandrasekhar, J.; Madura, J. D.; Impey, R. W.; Klein, M. L. Comparison of Simple Potential Functions for Simulating Liquid Water. *J. Chem. Phys.* **1983**, *79*, 926−935.
(54) Case, D. A.; Darden, T. A.; Cheatham, T. E., III; Simmerling, C. L.; Wang, J.; Duke, R. E.; Luo, R.; Walker, R. C.; Zhang, W.; Merz, K. M.; et al. *AMBER*; University of California: San Francisco, 2010.
(55) Darden, T.; York, D.; Pedersen, L. Particle Mesh Ewald: an $N\cdot\log(N)$ Method for Ewald Sums in Large Systems. *J. Chem. Phys.* **1993**, *98*, 10089−10092.
(56) Yang, S.; Cho, M. Direct Calculations of Vibrational Absorption and Circular Dichroism Spectra of Alanine Dipeptide Analog in Water: Quantum Mechanical/Molecular Mechanical Molecular Dynamics Simulations. *J. Chem. Phys.* **2009**, *131*, 135102.
(57) Abbate, S.; Longhi, G.; Kwon, K.; Moscowitz, A. The Use of Cross-Correlation Functions in the Analysis of Circular Dichroism Spectra. *J. Chem. Phys.* **1998**, *108*, 50−62.
(58) Oppenheim, A. V.; Schafer, R. W. *Discrete-Time Signal Processing*, 2nd ed.; Prentice-Hall: Upper Saddle River, NJ, 1999.
(59) Rhee, H.; Choi, J.-H.; Cho, M. Infrared Optical Activity: Electric Field Approaches in Time Domain. *Acc. Chem. Res.* **2010**, *43*, 1527−1536.
(60) Tych, K. M.; Burnett, A. D.; Wood, C. D.; Cunningham, J. E.; Pearson, A. R.; Davies, A. G.; Linfield, E. H. Applying Broadband Terahertz Time-Domain Spectroscopy to the Analysis of Crystalline Proteins: A Dehydration Study. *J. Appl. Crystallogr.* **2011**, *44*, 129−133.
(61) LaViolette, R. A.; Harris, R. A. Chiral Fluctuations in Achiral Clusters and Liquids Via Molecular Dynamics Simulations. *J. Chem. Phys.* **2002**, *116*, 7104−7108.